# Predictions of pre-edge features in time-resolved near edge X-ray absorption fine structure spectroscopy from hole-hole Tamm–Dancoff approximated density functional theory

*Edward G. Hohenstein,[1,2]* Jimmy K. Yu,[1,2,3] Christoph Bannwarth,[1,2] Nanna Holmgaard List,[1,2] Alexander C. Paul,[4] Sarai D. Folkestad,[4] Henrik Koch,[4,5] and Todd J. Martínez[1,2]*

[1]Department of Chemistry and The PULSE Institute, Stanford University, Stanford, CA 94305

[2]SLAC National Accelerator Laboratory, 2575 Sand Hill Road, Menlo Park, CA 94025

[3]Biophysics Program, Stanford University, Stanford, CA 94305

[4]Department of Chemistry, Norwegian University of Science and Technology, NTNU, 7491 Trondheim, Norway

[5]Scuola Normale Superiore, Piazza dei Cavaleri 7, 56126 Pisa, Italy

**Corresponding Author**

*E-mail: egh4@slac.stanford.edu

## ABSTRACT

Time-resolved near edge X-ray absorption fine structure (TR-NEXAFS) spectroscopy is a powerful technique for studying photochemical reaction dynamics with femtosecond time resolution. From the theoretical perspective, a unique challenge manifests in simulations of these experiments: to avoid ambiguity in the evaluation of the TR-NEXAFS spectrum from nonadiabatic dynamics simulations, core and valence-excited states must be evaluated on equal footing and those valence states must also define the potential energy surfaces used in the nonadiabatic dynamics simulation. In this work, we demonstrate that hole-hole Tamm–Dancoff approximated density functional theory (*hh*-TDA) is capable of directly simulating TR-NEXAFS spectroscopies. We apply *hh*-TDA to the excited-state dynamics of acrolein. We identify two pre-edge features in the oxygen K-edge TR-NEXAFS spectrum associated with the $S_2$ ($\pi\pi^*$) and $S_1$ ($n\pi^*$) excited states. Due to the low computational complexity and our GPU-accelerated implementation of *hh*-TDA, this method is promising for the simulation of pre-edge features in TR-NEXAFS spectra of large molecules and molecules in the condensed phase.


## TOC GRAPHICS

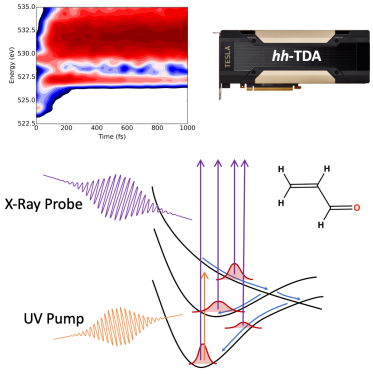



## KEYWORDS

NEXAFS, acrolein, excited-state dynamics, time-resolved spectroscopy

## INTRODUCTION

Time-resolved spectroscopies are indispensable tools for the experimental characterization of the ultrafast dynamics of organic molecules.[1] In the context of photochemistry, the most common of these techniques are pump-probe measurements where a pump pulse excites an electronic transition among valence electronic states and an optical probe pulse interrogates changes in vibrational or valence electronic levels. The development of X-ray free electron lasers enabled ultrafast time-resolved X-ray absorption and high-energy photoelectron spectroscopies with femtosecond time resolution.[2] These spectroscopies probe core-excited or ionized states and are complementary to the more traditional spectroscopies that use lower-energy probes.[3-4] By targeting core excitations, these spectroscopies offer element specificity and provide a means to probe the local chemical environment of those atoms.[5] This is especially powerful in organic molecules that may contain relatively few heteroatoms, which can be directly examined.[6-10]

From the theoretical perspective, there is a need to be able to predict time-resolved X-ray observables in order to aid in the assignment of these spectra as well as to make predictions that can be directly tested by time-resolved X-ray spectroscopies.[11-19] This is challenging for a variety of reasons — in this work, we will focus our discussion on the challenges associated with the simulation of organic molecules and photochemical processes initiated by pump pulses in the UV/visible region. First, the nonadiabatic dynamics of the molecules initiated by valence excitation must be simulated. While not at all unique to time-resolved X-ray spectroscopies, simulation of excited-state dynamics remains a formidable problem and necessitates electronic structure methods that are capable of accurately describing multiple electronic states across large regions of configurational space. These methods must be able to describe degeneracies between

electronic states (conical intersections) as well as bond breaking reactions.[20-22] Finally these methods must be highly efficient, so that the time-evolution of the nuclear wavepacket can be sampled sufficiently to resolve the observables of interest. The unique challenge of resonant X-ray probes is that, in addition to valence excitations, core excitations must also be described.[23-24]

In this context, a subtle, but important issue that is often overlooked is that if the core-excited states and the valence-excited states are described by different electronic structure methods, the evaluation of the X-ray absorption spectrum may become ambiguous.[25] The character of the valence states used in the dynamics simulation may differ from the character of those states obtained during the determination of the core-excited states as a result of such inconsistent treatment of the electronic structure. As long as transition matrix elements between the core-excited states and the valence states used in the dynamics simulation can be evaluated, the spectrum can be uniquely defined. The most straightforward way to guarantee that these matrix elements are available and well-behaved is to evaluate the core- and valence-excited states with the same method (i.e. ensuring that their wavefunctions are eigenfunctions of the same Hamiltonian). This ideal solution places additional demands on the electronic structure method, which must accurately reproduce not only the valence-excited state but also core-excited states.

Coupled-cluster theory provides some of the most accurate methods commonly applied to core-excited states.[26-33] When single and double excitations are included – as in equation-of-motion coupled-cluster singles and doubles (EOM-CCSD)[34] – K-edge transitions dominated by single-electron excitation character are within 1-2 eV of experimental values for organic molecules.[27-28] When approximate triple excitations are included, core excitation energies can be predicted with 0.1 eV accuracy provided corrections for relativistic effects are included.[35-37]

However, coupled-cluster methods are not ideally suited to applications in nonadiabatic dynamics due to their high computational expense, dependence on a single determinant reference state, and problems describing conical intersections between any pair of states.[38-40] Of the more traditional multireference methods, restricted active space (RAS) methods[41-43] are well suited to predictions of time-resolved X-ray observables.[44-48] With RAS orbital spaces, a complete active space (CAS) can be applied to the valence electronic states and nonadiabatic dynamics. Core excitations can be included with additional RAS orbital spaces that allow for single excitations from the core to virtual orbitals. In the context of restricted active space second-order perturbation theory (RASPT2),[41] both core and valence excitations can be treated with quantitative accuracy; however, one is still limited by the computational cost of this approach.[45-49] Less computationally demanding single-reference methods, such as time-dependent density functional theory (TD-DFT), do not provide a satisfactory description of the nonadiabatic dynamics among the valence electronic states.[50] Semi-empirical methods, that are often applied in a multireference framework to study photochemical processes,[51-55] typically do not explicitly include core electrons. Therefore, standard formulations of semiempirical methods are not applicable to the prediction of time-resolved X-ray observables.

Recently, we have developed a highly optimized graphical processing unit (GPU) accelerated implementation[56-57] of hole-hole Tamm–Dancoff approximated density functional theory (*hh*-TDA).[58-60] This method starts from a (*N*+2)-electron reference state and constructs ground and excited-state electronic wavefunctions by applying a pair of annihilation operators to this reference. In that way, the *hh*-TDA method is capable of describing excited electronic states involving transitions to the lowest unoccupied molecular orbital (LUMO). The advantage of this method is that, unlike TD-DFT, the ground and excited states are treated equivalently. As a

result, conical intersections between all pairs of states have the proper topology. Further, dynamic electron correlation is included through the exchange-correlation potential, rather than a wavefunction-based expansion; this provides quantitatively accurate excitation energies without significantly increasing the computational expense of the method. In practice, we find that the cost of our *hh*-TDA implementation scales as $O(N^2)$ with system size and is applicable to molecular systems with more than 2000 atoms. Of particular interest is the fact that *hh*-TDA performs well for low-lying valence states of both ππ* and nπ* character.[61] A feature of *hh*-TDA that has yet to be explored is its ability to describe the lowest few core-excited states – in particular, the states relevant to the pre-edge features that appear in time-resolved near edge X-ray absorption fine structure (TR-NEXAFS) spectroscopy.[35] In this context, the relevant core-excited states are dominated by single excitations to the LUMO and thus are captured by *hh*-TDA. Since the active orbital space in *hh*-TDA natively includes both core and valence orbitals, core-excited states are evaluated on equal footing with the valence-excited states and, therefore, a TR-NEXAFS spectrum can be computed from a nonadiabatic dynamics simulation using *hh*-TDA potential energy surfaces without ambiguity.

In this work, we test the ability of *hh*-TDA to describe the X-ray absorption of several small molecules at the carbon, nitrogen and oxygen K-edges. In particular, we emphasize predictions of pre-edge features relevant to TR-NEXAFS spectroscopy due to excited-state absorption from low-lying electronic states. We consider the TR-NEXAFS spectrum of acrolein at the oxygen K-edge in more detail. Acrolein is the simplest unsaturated aldehyde and provides a prototypical example of photodynamics involving both ππ* and nπ* excited states.[62] After benchmarking the performance of *hh*-TDA for the core and valence states of acrolein, we perform an *ab initio* multiple spawning (AIMS) simulation to model the photodynamics initiated

by excitation of the ππ* transition. Subsequently, we predict the resulting TR-NEXAFS spectrum using *hh*-TDA.

## THEORETICAL METHODS

The *hh*-TDA[58-59] computations in this work were performed using the GPU-accelerated quantum chemistry package TeraChem.[63-66] These computations use the ωPBEh exchange correlation functional[67] with a range separation parameter of 0.3 $bohr^{-1}$ and a 0.3 fraction of full-range Hartree–Fock (exact) exchange; these computations use the 6-31G** basis set. The AIMS simulation[68] of acrolein was initialized with 30 trajectory basis functions on the $S_2$ state; during the course of the simulation an additional 805 trajectory basis functions were spawned. The initial positions and momenta of these functions were obtained by sampling a Wigner distribution at 0K of the ground state harmonic vibrational wavefunction of acrolein computed at the *hh*-TDA/6-31G** level of theory (employing the modified ωPBEh functional described above). All AIMS trajectory basis functions were propagated in time for 1 ps using 0.5 fs time steps or until the norm of the population of that basis function fell below 0.01. Upon reaching the ground electronic state, trajectory basis functions were propagated on the Kohn-Sham ωPBEh potential surface.

The simulated TR-NEXAFS spectrum of acrolein was produced within a fully incoherent approximation by computing both the core- and valence-excited states with *hh*-TDA at the centroid of each trajectory basis function every 10 fs; more than 41000 single point calculations of the core-excited states were included in the simulated TR-NEXAFS spectrum. The contributions from each of these points are weighted by the norm of the corresponding AIMS wavefunction coefficient and the oscillator strength with the relevant valence electronic state.

The resulting time-resolved spectrum was convolved with Gaussian functions having full-width at half max of 0.25 eV in energy (to smooth the data) and 50 fs in time (to simulate the instrument response function). Note that a spectrum computed in this way includes only contributions from initially photoexcited molecules, or equivalently, assumes an excitation fraction of 1. This is sufficient to characterize the time-dependence of the pre-edge features in the TR-NEXAFS spectrum that are of interest in this case.

The accuracy of *hh*-TDA was compared to coupled-cluster methods (CCSD and CC3) for the carbon K-edges of acrolein and malonaldehyde, the nitrogen K-edges of 2,3-diazabutadiene and azobenzene, and the oxygen K-edges of acrolein, malonaldehyde and uracil. The geometry of each of the molecules utilized in this analysis can be found in the Supporting Information. Half of the geometries are equilibrium geometries (in the case of acrolein and malonaldehyde) and the remaining structures are near-equilibrium structures sampled from a Wigner distribution of the ground state harmonic vibrational wavefunction at the equilibrium geometry. The geometries (and vibrational wavefunctions) were obtained from optimizations with DFT using the functionals chosen for subsequent *hh*-TDA computations. The CC3 computations[69-70] were performed using the $e^{T}$ electronic structure program.[71] Equation of motion (EOM) transition properties between valence and core-excited states were computed using core-valence separation (CVS) approximation,[23, 29, 72] with a local development branch of the code. An aug-cc-pCVTZ basis for the atom associated with the K-edge of interest and an aug-cc-pVTZ basis was used for the remaining atoms; we denote this basis as aug-cc-p(C)VTZ. CCSD computations were performed in a similar manner using TeraChem.[73] In the case of CCSD computations on azobenzene, the aug-cc-pCVDZ basis set was used for all atoms.

**RESULTS & DISCUSSION**

***Comparison of hh-TDA to CC3***

In the *hh*-TDA method, all core and valence molecular orbitals are treated on equal footing since they appear as doubly occupied orbitals in the (*N*+2)-electron reference state. Annihilation of core electrons leads to singly and doubly excited configurations in the *hh*-TDA expansion that describe core excitations. The primary limitation of this approach is the restrictive nature of the unoccupied space – that is, only excitations to the LUMO are allowed. We have shown previously that *hh*-TDA is capable of accurately describing the lowest few electronic excited states in a variety of photoactive molecules.[56] Since core excitations to the LUMO are also included in the *hh*-TDA expansion, low-lying core-excited states can also be described. The remaining question is how accurate this description will be.

To begin, we should place some expectations on what *hh*-TDA is capable of describing in the context of core excitations. Due to the severe limitations on the unoccupied space in the *hh*-TDA method, it is unreasonable to expect an accurate prediction of the X-ray absorption spectrum over a large range of wavelengths. It is only the first few contributions to this spectrum that will be accessible. At best, it is only one core-excited state per core orbital at a given K-edge can be treated reasonably (i.e. all the single excitations from the core orbitals to the LUMO). At higher energies, core excitations involving higher-lying virtual orbitals as well as doubly-excited states involving one valence and one core excitation appear; the excitations involving the LUMO+*n* virtual orbital (with $n>0$) simply do not appear in *hh*-TDA. While doubly excited states do appear, they are restricted to those including a doubly-occupied LUMO. As a result, we suggest that only single core excitations involving the LUMO be considered. While this has limited utility in the context of modelling X-ray absorption spectroscopy in general, it can still be quite powerful in the context of time-resolved X-ray absorption. This is because the transient

pre-edge features characteristic of valence-excited states can often be accurately described through the inclusion of only the lowest few core-excited states. It is common that the most intense pre-edge features result from transitions between a valence-excited state and a core excitation to the LUMO.[35] Therefore, in this work, we will focus on the ability of *hh*-TDA to predict these pre-edge features as well as the direct prediction of TR-NEXAFS observables.

In Figures 1 – 6, we compare the X-ray absorption spectrum at the oxygen K-edge (Figures 1 and 2), nitrogen K-edge (Figures 3 and 4) and carbon K-edge (Figures 5 and 6) predicted by CC3 and *hh*-TDA for several small organic molecules. In each case, we consider absorption from the ground state as well as excited-state absorption from the first two valence-excited states. Since what is most important in this comparison is the relative position of the pre-edge features, we apply a rigid shift to all *hh*-TDA core excitation energies to align the spectrum with the first core excitation from the ground state. For each molecule, an exchange-correlation functional that performs well in the description of the valence states is chosen. In our previous work, we have explored the effect of the choice of exchange-correlation functional in the context of *hh*-TDA.[56-57]

The X-ray absorption at the oxygen K-edge of malonaldehyde and uracil is shown in Figures 1 and 2, respectively. The *hh*-TDA computations on malonaldehyde use the ωB97 functional, while the computations on uracil use the ωPBE functional with a range separation parameter of 0.2 au. Both of these functionals have been previously validated for their ability to describe the valence states of these molecules.[56] In the case of malonaldehyde *hh*-TDA performs quite well in its description of the absorption from all three of the electronic states considered. Malonaldehyde, at its $S_0$ minimum, has two inequivalent oxygen atoms from which to excite. There is generally good agreement between CC3 and *hh*-TDA in the relative intensities and

splittings of these two resulting peaks. However, the splittings predicted by *hh*-TDA are not quite as large as those described by CC3. Further, the oscillator strengths associated with absorption from the ground state are somewhat underestimated relative to CC3. In all, the predictions made with *hh*-TDA are quite reasonable and capture the pre-edge features of the X-ray absorption spectrum. The structure of the X-ray absorption spectrum of uracil is much simpler than that of malonaldehyde. The pre-edge is dominated by a single peak resulting from excited-state absorption from the $S_1$ $n\pi^*$ state. This feature is reproduced by *hh*-TDA and there is good agreement between CC3 and *hh*-TDA in both the location and oscillator strength of that peak. Again, the oscillator strength of the ground state absorption is significantly underestimated (here by roughly a factor of 2). In contrast, the oscillator strength of the excited-state absorption from the $S_2$ $\pi\pi^*$ state is somewhat overestimated by *hh*-TDA – although it remains significantly weaker than absorption from the $S_1$ state. There is also good agreement between CC3 and *hh*-TDA in the location of the absorption peaks from the $S_2$ state. For both malonaldehyde and uracil, *hh*-TDA is capable of reproducing the pre-edge features predicted by CC3 in the X-ray absorption spectrum at the oxygen K-edge.

In Figures 3 and 4, the X-ray absorption at the nitrogen K-edge of 2,3-diazabutadiene and azobenzene is shown. For 2,3-diazabutadiene, the ωPBEh functional with a modified range separation parameter of 0.55 au was used. For azobenzene, the BHLYP functional is used and the molecular orbitals are determined from an *N*-electron ensemble Hartree–Fock computation with the electrons evenly distributed in *N*/2+1 orbitals.[57, 61] The performance of *hh*-TDA is similar for these molecules as it was at the oxygen K-edge of malonaldehyde and uracil. For 2,3-diazabutadiene, the primary contribution in the pre-edge region is due to excited-state absorption from the $S_1$ $n\pi^*$ state. Less prominent features due to excited-state absorption from the $S_2$ $\pi\pi^*$

state are seen at slightly lower as well as slightly higher energies than the peak originating from $S_1$. There is good agreement between CC3 and *hh*-TDA in the location and intensity of the lowest energy peaks originating from $S_1$, while the location of the $S_2$ peaks are blue-shifted by roughly 1 eV by *hh*-TDA relative to CC3. There is disagreement between CC3 and *hh*-TDA regarding the higher energy peaks due to excited-state absorption from $S_2$. CC3 predicts several peaks with very low intensity between 394 eV and 397 eV; *hh*-TDA predicts a single much more intense peak at about 397 eV. This peak involves a final state characterized by a doubly excited configuration, (N 1s$\rightarrow\pi^*$)(n$\rightarrow\pi^*$). We note, however, that in experiment, it is likely that the two lowest energy peaks would provide the best signatures for the $S_1$ and $S_2$ states, since they are further separated from any ground state absorption. For azobenzene, we compare *hh*-TDA to CCSD due to the expense associated with a CC3 computation of the larger molecule. Unlike 2,3-diazabutadiene, CCSD predicts that the pre-edge X-ray absorption at the nitrogen K-edge of azobenzene contains only a single significant contribution: a strong excited-state absorption feature from the $S_1$ n$\pi^*$ state (two nearly degenerate core-excited states contribute to this feature). Both CCSD and *hh*-TDA predict that absorption from the $S_2$ $\pi\pi^*$ state is quite weak. As was the case at the oxygen K-edge, *hh*-TDA seems to underestimate the oscillator strength of ground state absorption by as much as a factor of 2. Again, it appears that *hh*-TDA provides a suitably accurate description of the pre-edge X-ray absorption features of both 2,3-diazabutadiene and azobenzene.

Finally, we consider X-ray absorption at the carbon K-edge of acrolein and malonaldehyde. For acrolein, a modified ωPBEh functional with a range separation parameter of 0.3 au and a 0.3 fraction of full-range exact exchange is applied in the *hh*-TDA computations. For malonaldehyde, the ωB97 functional is again used. Each of these molecules contains three

carbon atoms and, therefore, three excitations from carbon 1*s* core orbitals to the LUMO. We find *hh*-TDA to be much less suitable for the prediction of spectra at the carbon K-edge than it was for X-ray absorption at both the nitrogen and oxygen K-edges. For acrolein, the pre-edge region of the spectrum is qualitatively different as described by CC3 and *hh*-TDA. CC3 predicts a weak, single peak at 278 eV due to two nearly degenerate core-excited states. With *hh*-TDA, these states are split by more than 1 eV and the oscillator strength with $S_2$ is increased. More damaging is the prominent pre-edge feature predicted by *hh*-TDA to appear at 283 eV resulting from excited-state absorption from $S_1$ that is not present when the absorption is treated with CC3. As a result, *hh*-TDA does not adequately describe the pre-edge region at the carbon K-edge of acrolein. The performance of *hh*-TDA is better for malonaldehyde simply because no spurious contributions to the spectrum appear. There is reasonable agreement between CC3 and *hh*-TDA that excited-state absorption from $S_2$ results in a feature at roughly 280 eV. Similarly, both methods agree that a second, less intense feature appears at roughly 281 eV due to excited state absorption from $S_1$. However, in this case, the ground state absorption spectrum is significantly different as predicted by CC3 and *hh*-TDA; *hh*-TDA predicts three core excited states to be within 0.4 eV of each other – this gives rise to the single absorption peak at 287.5 eV. In contrast, CC3 predicts two nearly degenerate states at 287 eV and a single state with lower energy at 285 eV – this lower energy state also has a much lower oscillator strength with the ground state. On the basis of these results, we cannot recommend *hh*-TDA for use in simulating X-ray absorption at the carbon K-edge.

To understand the failings of *hh*-TDA at the carbon K-edge, we have considered the case of acrolein in more detail. These results can be found in the Supporting Information. We find that with *hh*-TDA the splittings between core-excited states are largely governed by the orbital

energies. The double anion ωPBEh reference splits each of the carbon 1s orbital energies by roughly 1 eV and this directly manifests in the *hh*-TDA excitation energies. In contrast, EOM-CCSD using those same orbitals will behave almost identically (in terms of splittings) to a canonical EOM-CCSD computation using the Hartree–Fock orbitals of a neutral molecule. This can be seen in the diagonal matrix elements of the *hh*-TDA Hamiltonian and EOM-CCSD similarity transformed Hamiltonian (i.e. the three matrix elements describing a (C 1s→π*) excitation). The splittings obtained from consideration of these diagonal matrix elements are qualitatively similar to the final excitation energies – that is even at the level of the matrix elements, EOM-CCSD predicts two nearly degenerate core excitations and a third that is higher in energy by about 1.7 eV as opposed to 1.4 eV from the full EOM-CCSD computation. For *hh*-TDA, the three low-lying states are separated by 0.7 and 1.1 eV, respectively; in the full *hh*-TDA computation, the analogous splittings are 1.4 and 0.8 eV. This is primarily a demonstration that coupled-cluster methods are less sensitive to the choice of molecular orbitals than a method like *hh*-TDA with limited variational flexibility.

Another issue with *hh*-TDA is the restriction of the virtual space to the LUMO; again we will consider the specific case of the carbon K-edge of acrolein. We have explored the effect of this limitation by recognizing that *hh*-TDA based on a Hartree-Fock reference is exactly equivalent to a complete active space configuration interaction (CASCI) computation using Hartree-Fock orbitals and an active space with 30 electrons in 16 orbitals (in the case of acrolein). From the CASCI perspective, we can expand the active space to include an additional virtual orbital (i.e. 30 electrons in 17 orbitals). We find that this extension does not significantly improve the excitation energies, but does increase the oscillator strengths. We have noted a systematic underestimation of the oscillator strengths for all core excitations from the ground

state relative to the oscillator strengths predicted by CCSD and CC3. We attribute this underestimation to the lack of flexibility in the virtual space. By comparing the natural transition orbitals obtained from CCSD and *hh*-TDA, we see that the particle orbitals obtained from CCSD tend to localize somewhat around the hole state. In contrast, *hh*-TDA lacks the variational flexibility for such localization and the particle orbitals are all indistinguishable from (but not identical to) the LUMO.

From the comparison between *hh*-TDA and CC3, there are a few general conclusions that can be drawn. First, the oscillator strength associated with absorption from the ground state is systematically underestimated by *hh*-TDA. In contrast, both the relative energy and oscillator strength of excited-state absorption from states with nπ* character is accurately captured. The relative energy of excited-state absorption peaks from states with ππ* character are also well described, but the oscillator strengths are somewhat overestimated. Also in the context of excited state absorption from states with ππ* character, the lowest energy peak(s) associated with core to LUMO single excitations are well described, however, higher energy peaks – still in the pre-edge region of the spectrum – are either absent or poorly described. The X-ray absorption spectra at the nitrogen and oxygen K-edges are predicted accurately by *hh*-TDA; the carbon K-edge is not as well described. As a general rule, *hh*-TDA can probably be applied in most cases where a small number (i.e. one or two) heteroatoms contribute to the X-ray absorption spectrum at a given edge. In cases where larger numbers of atoms contribute (i.e. at the carbon K-edge), inaccuracies begin to manifest as a result of the limited virtual space and lack of orbital relaxation in *hh*-TDA.

***Photodynamics and TR-NEXAFS of Acrolein***

To demonstrate the use of hh-TDA for in-silico TRXAS experiments, we consider the photodynamics of s-*trans* acrolein initiated by a UV pump resonant with the ππ* transition to its $S_2$ state. The $S_1$ state of acrolein is a low-lying nπ* excited state. This nπ* state can be pumped directly and has an excited-state lifetime on the order of 2 ps (on the basis of cavity ringdown measurements).[74] However, when the ππ* transition of acrolein is pumped, time-resolved photoelectron spectroscopy (TRPES) shows a bi-exponential decay with a fast component on the order of 100 fs and a slow component of 900 fs.[75] The fast component is assigned to the deactivation of the $S_2$ state and the slow component is assigned to the recovery of the ground state from a minimum on the $S_1$ state. This molecule is a good candidate for TR-NEXAFS because a distinctive pre-edge feature associated with the $S_1$ minimum (which has nπ* character) should be observable.

As with all DFT methods, the accuracy of *hh*-TDA is inextricably linked to the selection of exchange-correlation functional. As a result, calibration against experiment and accurate *ab initio* methods is essential. We benchmark the performance of *hh*-TDA using the ωPBEh functional[67] for its ability to describe the lowest two valence states of acrolein in Table 1. We have found that ωPBEh provides accurate results and allows for some degree of "tuning" through the range separation parameter and fraction of full-range Hartree–Fock exchange that is included. For acrolein, *hh*-TDA with ωPBEh is in excellent agreement with wavefunction-based *ab initio* methods and experiment in the prediction of the excitation energy to the $S_1$ and $S_2$ states at the Franck–Condon point. It is also in quantitative agreement with experiment in the energy of the $S_1$ minimum relative to the Franck–Condon point. We compare the relative energies of the minimum energy conical intersections (MECIs) to SA-CASSCF and find reasonable agreement in the energetics of these intersections between *hh*-TDA and SA-CASSCF. We find *hh*-TDA to

perform well relative to high-level CC3/aug-cc-p(C)VTZ performed at the *hh*-TDA optimized geometries; the vertical excitation energies and the adiabatic excitation to the $S_1$ minimum show good agreement between *hh*-TDA and CC3. The relative energies of the conical intersections appear to be somewhat underestimated by *hh*-TDA relative to CC3, this might lead *hh*-TDA to predict additional trapping of the wavepacket in this minimum. However, the CC3 computations are performed at the *hh*-TDA MECIs and the energies are obtained by averaging the upper and lower states, the underestimation of this barrier may be an artifact of this averaging. This comparison indicates that *hh*-TDA is suitable to describe the regions of the potential energy surfaces relevant to the photodynamics of s-*trans* acrolein.

The lifetimes of the singlet excited states of s-*trans* acrolein following excitation to the $S_2$ electronic state obtained from our AIMS simulation are presented in Figure 7. We characterize the observed population dynamics using delayed (bi-)exponential functions.

$$P(t) = \begin{cases} 1 & t < t_0 \\ ce^{(t+t_0)/\tau_1} + (1-c)e^{(t+t_0)/\tau_2} & t \geq t_0 \end{cases} \tag{1.1}$$

Here, the $t_0$ parameter represents the onset time of the decay; physically, the onset time characterizes the delay between photoexcitation and the time at which the nuclear wavepacket begins to reach a conical intersection. The $\tau$ parameters quantify the rates of population transfer that occurs once the wavepacket has reached an intersection. We find that the decay of the $S_2$ state is well described by a delayed exponential (where $c = 1$). The associated lifetime of about 100 fs is within the experimental error bars of the fast decay components associated with TRPES experiments.[75] The recovery of the ground state, however, exhibits bi-exponential behavior. In this case, there is a fast component of 90 fs and a slow component of 1.1 ps (in addition to the onset time of about 50 fs). The fast component accounts for about 70% of the population

transfer. This indicates that the wavepacket decays rapidly from $S_2$ to $S_1$ through a conical intersection; subsequently, the wavepacket splits and 70% directly decays to the ground state through a nearby intersection between $S_0$ and $S_1$. The remaining 30% of the wavepacket is trapped in the minimum on $S_1$ and eventually decays back to $S_0$ with a time constant of 1.1 ps. In both cases, the decay to the ground state is through the same region of the intersection seam characterized by a 90° twist of the $CH_2$ group. This slow component of the decay also seems to agree reasonably well with TRPES measurements that predict a slow decay component of 900±100 fs.[75] Although this apparent agreement inspires some confidence that *hh*-TDA accurately predicts the excited-state lifetimes, to make a more definitive comparison with this experiment, the TRPES observable would need to be computed directly.

In Figure 8, we show the oxygen K-edge absorption spectra of the $S_0$, $S_1$, and $S_2$ states at the Franck–Condon point. Experimentally, the oxygen 1s to π* excitation is found at 531 eV. On the basis of *hh*-TDA and CC3 computations, we predict a prominent pre-edge feature to appear at 527 eV associated with the excited state of nπ* character. Based on the involvement of the $S_1$ minimum observed in the AIMS simulation, this pre-edge feature should be visible for longer than 1 ps. A less prominent feature associated with excited-state absorption from the ππ* $S_2$ state should appear at 524 eV. This feature, however, should be short lived due to the relatively short (100 fs) lifetime of the $S_2$ state. We find generally good agreement between *hh*-TDA and CC3 in their treatment of the K-edge absorption spectra. This is because a single core-excited state (the 1s to π* excitation) is responsible for the pre-edge features. The largest discrepancy (relevant to the TR-NEXAFS observable) between CC3 and *hh*-TDA is in the location of the second peak resulting from absorption from the $S_2$ state; CC3 predicts that this peak will be less intense and occur at 528 eV as opposed to *hh*-TDA which predicts more intense absorption occurring at

529.5 eV. In either case, it is the first peak (at 524 eV) that we expect to provide better signature of the $S_2$ state experimentally due to the lack of background in that region. The *hh*-TDA excitation energies at the oxygen K-edge are qualitatively correct, but red-shifted by 10 eV relative to experiment; errors of this size for core excitations are common for methods based on DFT.[32] In contrast, CC3 produces results that are quantitatively accurate (within 0.25 eV of experiment).

The simulated TR-NEXAFS spectrum at the oxygen K-edge of acrolein is presented in Figure 9. The dominant feature of this spectrum is the recovery of ground state absorption. This occurs at and above the oxygen K-edge. Here, it begins at roughly 530 eV and extends to higher energies. The pre-edge features that were predicted (see Figure 8) are all visible in the simulated TR-NEXAFS spectrum. The most prominent pre-edge feature (at 527 eV results from the population trapped in the $S_1$ minimum. In this minimum, the electronic wavefunction has $n\pi^*$ character with the nonbonding orbital localized on the oxygen atom before the probe pulse arrives; as a result, this state has a significant transition dipole moment (and, therefore, oscillator strength) with the lowest core-excited state at the oxygen K-edge. This pre-edge feature should be clearly identifiable in a TR-NEXAFS spectrum of acrolein and provide an unambiguous means of validating our simulation against experiment. The two pre-edge features associated with absorption from $S_2$ are also visible; however, the higher energy absorption at 529 eV is somewhat obscured by absorption from the ground state. On the basis of the CC3 computations, we expect that the feature at 529 eV is blue shifted by *hh*-TDA and that it will appear at 528 eV in experiment. Although less pronounced in the spectrum and relatively short-lived, the pre-edge feature at 524 eV visible at short time delays can be attributed to the wavepacket on the $S_2$ state leaving the Franck–Condon region. As the time resolution and sensitivity of TR-NEXAFS

spectroscopy improves (in concert with advancements in the development of X-ray free electron lasers), it may become possible to identify these weaker transient features of TR-NEXAFS spectra (our simulation predicts the pre-edge feature associated with the $S_1$ minimum to be 5 times more intense than the feature associated with the $S_2$ state). We have extracted lineouts from the spectrum at 524 and 527 eV and fit a sequential kinetics model to find a time constant of 20 fs for the decay of the signal at 524 eV; we find time constants of 70 and 440 fs for the rise and decay of the signal at 527 eV, respectively. This analysis is shown in Figure 10. The prediction of these time constants can be directly tested by experiment.

## CONCLUSIONS

Excited-state nonadiabatic dynamics simulations are powerful tools for understanding photochemical processes in atomistic detail. As with any simulation, however, validation against experimental observations is essential. Therefore, it is important to be able not only to perform nonadiabatic dynamics simulations, but also to provide experimentally testable observables along with the atomistic details of the dynamics. This way, the predictions made by simulations can be directly compared to the experiment. Here, we have demonstrated that the *hh*-TDA method is capable of generating accurate potential energy surfaces on-the-fly for use in trajectory based nonadiabatic dynamics simulations (e.g. AIMS) and also allows the TR-NEXAFS spectrum associated with the dynamics to be directly evaluated. This method has the further advantage that the TR-NEXAFS spectrum can be produced without the ambiguities that arise when different electronic structure methods are used to treat the valence states and the core-excited states.

The *hh*-TDA method appears to be suitable for simulating pre-edge features in TR-NEXAFS spectra of organic molecules at the nitrogen and oxygen K-edge as long as *hh*-TDA provides a suitably accurate description of the valence states. The restricted orbital space employed in *hh*-TDA limits the applicability of the method to molecules where only excitations to the LUMO dominate the nonadiabatic dynamics among valence states. The pre-edge features of a TR-NEXAFS spectrum of such molecules are dominated by excited state absorption features characterized as excitations from the 1s orbitals to the empty π or n orbitals. Therefore, despite the restricted orbital space of *hh*-TDA, it remains possible to describe the core-excited states relevant to the pre-edge features of TR-NEXAFS spectra. Therefore, we expect that the nitrogen and oxygen K-edge TR-NEXAFS spectra will be reasonably modeled by *hh*-TDA in most cases where *hh*-TDA also provides an accurate description of the valence states.

Owing to our GPU accelerated implementation of *hh*-TDA, this method can be routinely applied in nonadiabatic dynamics simulations. We consider the acrolein molecules a prototypical example to demonstrate *hh*-TDA used in AIMS simulations and predict the TR-NEXAFS spectrum. We were able to identify distinct features in the spectrum characterizing transitions between the lowest three valence states. Since no such experimental TR-NEXAFS spectrum exists in the literature at this point, this marks a true prediction, which may be challenged by future experiments. In addition to simulations of single molecules in the gas phase, our implementation of *hh*-TDA exhibits apparent quadratic computational complexity (O($N^2$) scaling), therefore it is applicable to photochemical processes involving larger molecules in the condensed phase, while still providing access to TR-NEXAFS observables. We believe this will be useful in the context of soft X-ray absorption experiments at the nitrogen and oxygen K-edge

of organic molecules in the liquid phase enabled by the next generation of X-ray free electron lasers.[3, 76]

## ASSOCIATED CONTENT

The following files are available free of charge.

A supplemental file is provided containing the molecular geometries obtained in this work and details of the coupled-cluster computations.

## AUTHOR INFORMATION

**Corresponding Author:** *E-mail: egh4@slac.stanford.edu

**Notes:** TJM is co-founder of PetaChem, LLC.

## ACKNOWLEDGMENT

This work was supported by the AMOS program of the U.S. Department of Energy, Office of Science, Basic Energy Sciences, Chemical Sciences, and Biosciences Division and by the Department of Energy, Laboratory Directed Research and Development program at SLAC National Accelerator Laboratory, under contract DE-AC02-76SF00515. CB was supported by the German National Academy of Sciences Leopoldina through the Leopoldina Fellowship Program (Project No. LPDS 2018-09). HK acknowledges funding from the Marie Skłodowska-Curie European Training Network ``COSINE – COmputational Spectroscopy In Natural sciences and Engineering", Grant Agreement No. 765739 and the Research Council of Norway through FRINATEK projects 263110 and 275506. The authors thank Dr. Thomas Wolf for helpful discussions.

**Table 1.** Energies of the $S_1$ and $S_2$ states of acrolein relative to the $S_0$ state at the Franck–Condon geometry in electronvolts.

| | *hh*-TDA[a] | Experiment | CC3[d] | SA-CASSCF[e] | SAC-CI[f] | CASPT2[g] |
|---|---|---|---|---|---|---|
| $S_2$ FC | 6.91 | 6.42[b] | 6.65 | 7.55 | 6.92 | 6.94 |
| $S_1$ FC | 3.85 | 3.77[b] | 3.70 | | 3.83 | 3.63 |
| $S_2/S_1$ MECI | 4.97 | n/a | 4.16 | 5.38 | n/c | n/c |
| $S_1$ Min | 3.23 | 3.21[c] | 3.30 | 2.96 | n/c | n/c |
| $S_1/S_0$ MECI | 3.91 | n/a | 3.54 | 3.94 | n/c | n/c |

[a] *hh*-TDA/6-31G** using the ωPBEh functional with a range separation parameter of 0.3 a.u. and 30% full-range Hartree–Fock exchange. This work. [b] Reference [77]. [c] References [78] and [79]. [d] CC3 computations use an aug-cc-p(C)VTZ basis set and are evaluated at *hh*-TDA optimized geometries; energies at the conical intersections are taken as the average of the upper and lower states. [e] State-averaged complete active space self-consistent field averaged over 3 states, using an active space with 6 electrons in 5 orbitals and a 6-31G* basis set, Reference [75]. [f] Symmetry adapted cluster configuration interaction, Reference [25]. [g] Complete active space second-order perturbation theory, Reference [80].

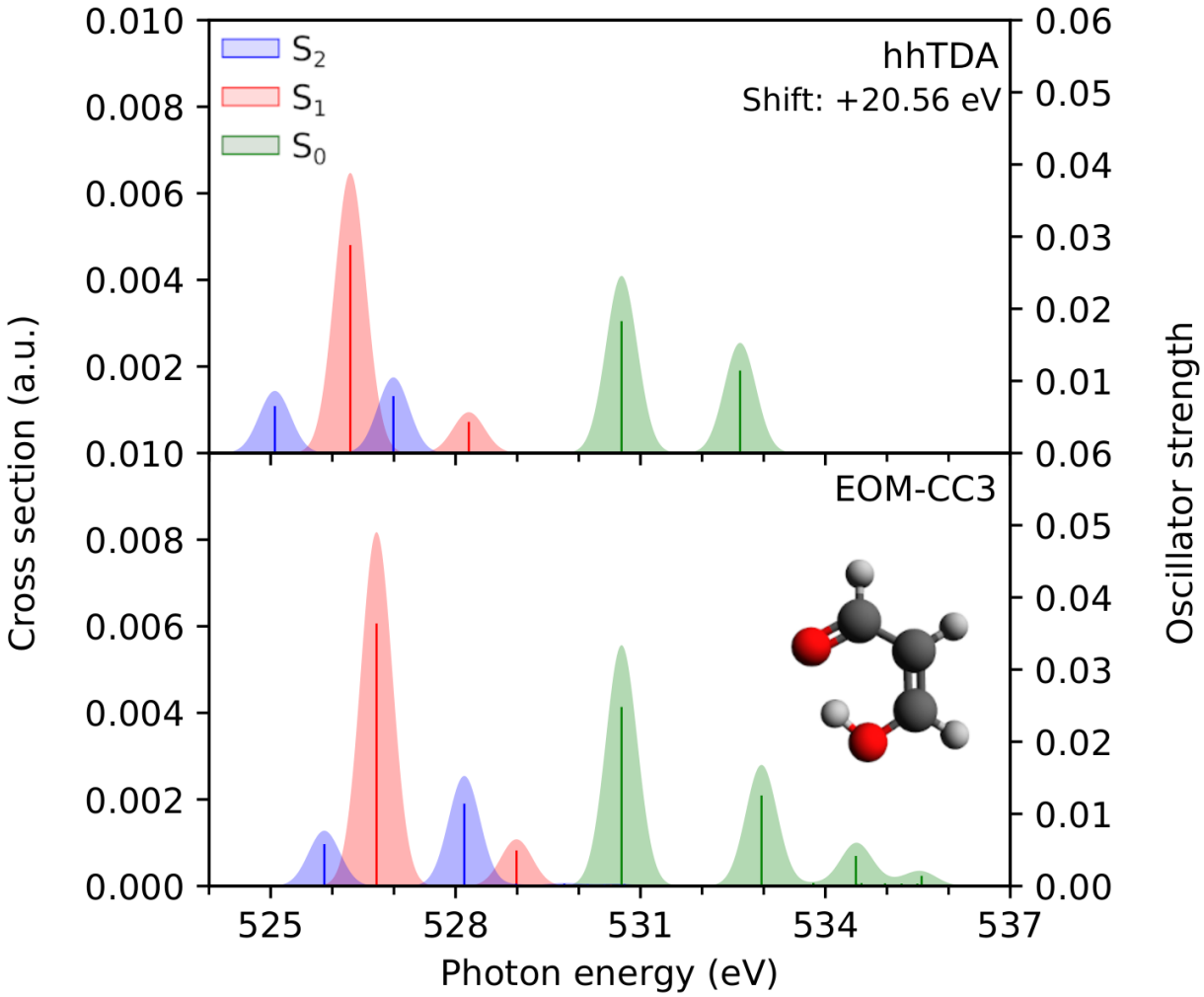


**Figure 1.** Comparison of X-ray absorption at the oxygen K-edge of malonaldehyde computed with (a) CC3/aug-cc-p(C)VTZ and (b) *hh*-TDA/cc-pCVDZ. Spectra are broadened with a Gaussian lineshape with full-width half maximum of 0.6 eV. The core-excitation energies are computed at the $S_0$ minimum geometry of malonaldehyde (in green). In blue and red, respectively, the excited-state absorption from the $S_1$ and $S_2$ states is shown. The *hh*-TDA excitation energies are shifted so that the first core excitation from the $S_0$ state between *hh*-TDA and CCSD is brought into agreement.

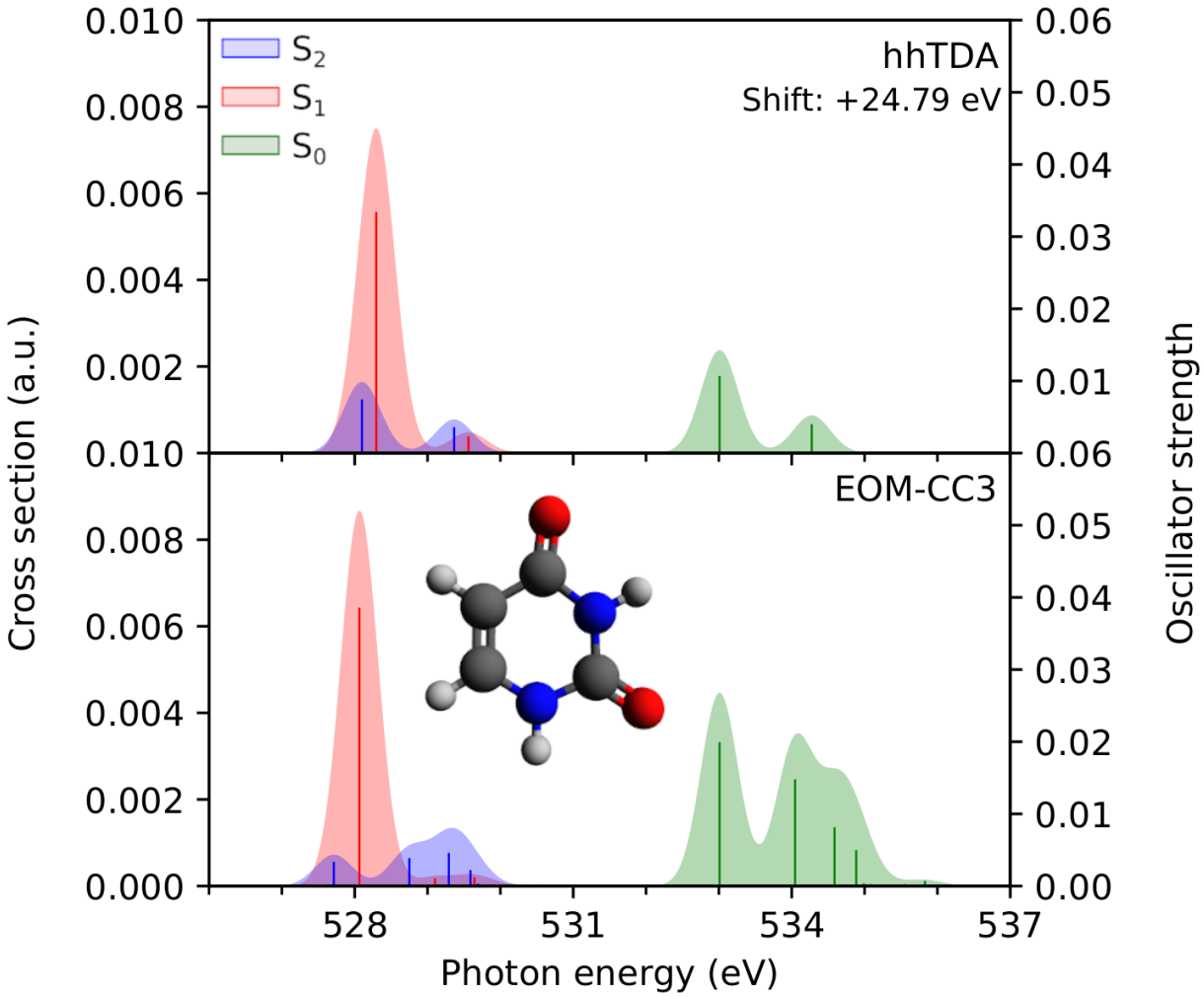


**Figure 2.** Comparison of X-ray absorption at the oxygen K-edge of uracil computed with (a) CC3/aug-cc-p(C)VTZ and (b) *hh*-TDA/cc-pCVDZ. Spectra are broadened with a Gaussian lineshape with full-width half maximum of 0.6 eV. The core-excitation energies are computed at the $S_0$ minimum geometry of uracil (in green). In blue and red, respectively, the excited-state absorption from the $S_1$ and $S_2$ states is shown. The *hh*-TDA excitation energies are shifted so that the first core excitation from the $S_0$ state between *hh*-TDA and CCSD is brought into agreement.

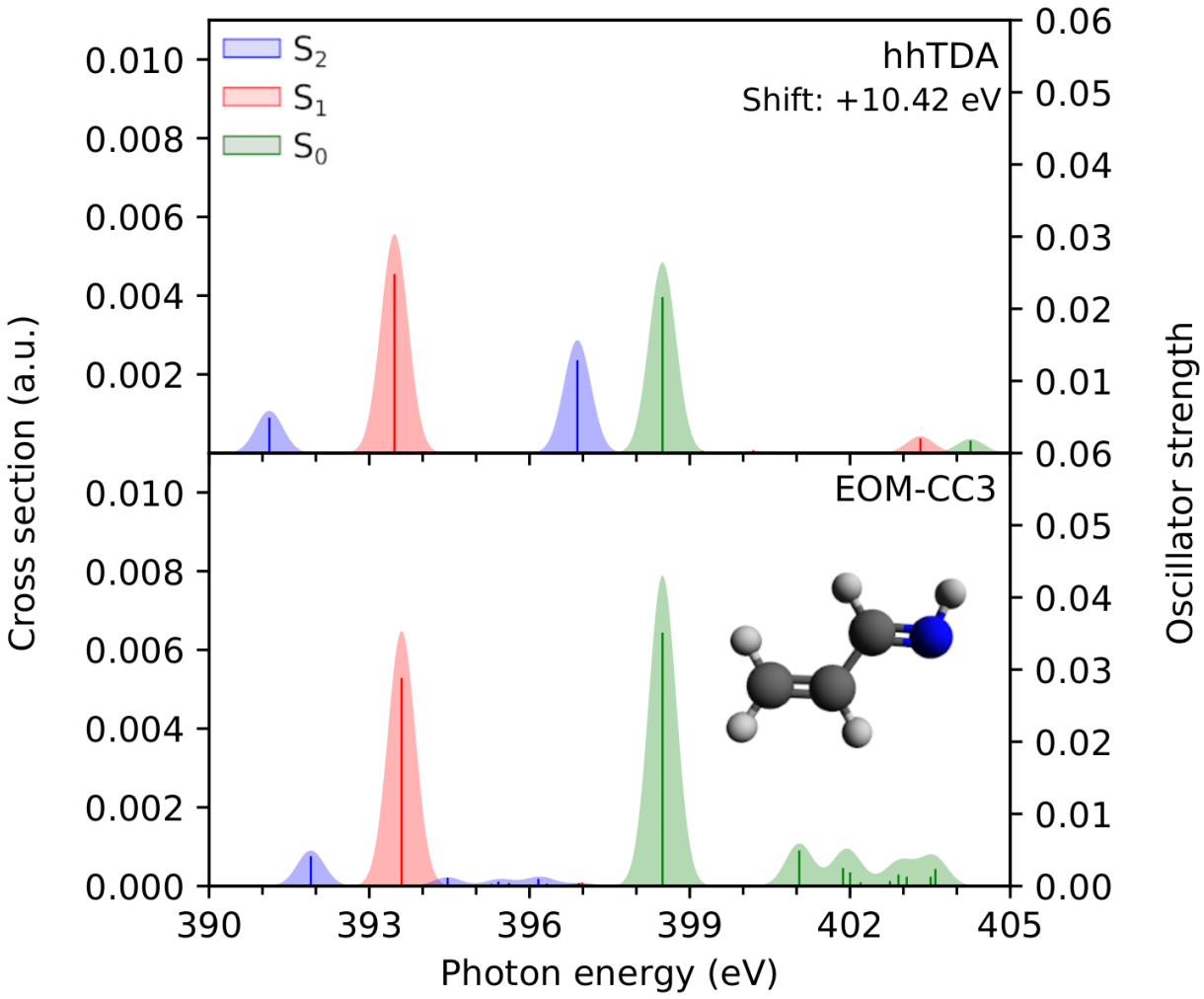


**Figure 3.** Comparison of X-ray absorption at the nitrogen K-edge of 2,3-diazabutadiene computed with (a) CC3/aug-cc-p(C)VTZ and (b) *hh*-TDA/cc-pCVDZ. Spectra are broadened with a Gaussian lineshape with full-width half maximum of 0.6 eV. The core-excitation energies are computed at the $S_0$ minimum geometry of 2,3-diazabutadiene (in green). In blue and red, respectively, the excited-state absorption from the $S_1$ and $S_2$ states is shown. The *hh*-TDA excitation energies are shifted so that the first core excitation from the $S_0$ state between *hh*-TDA and CCSD is brought into agreement.

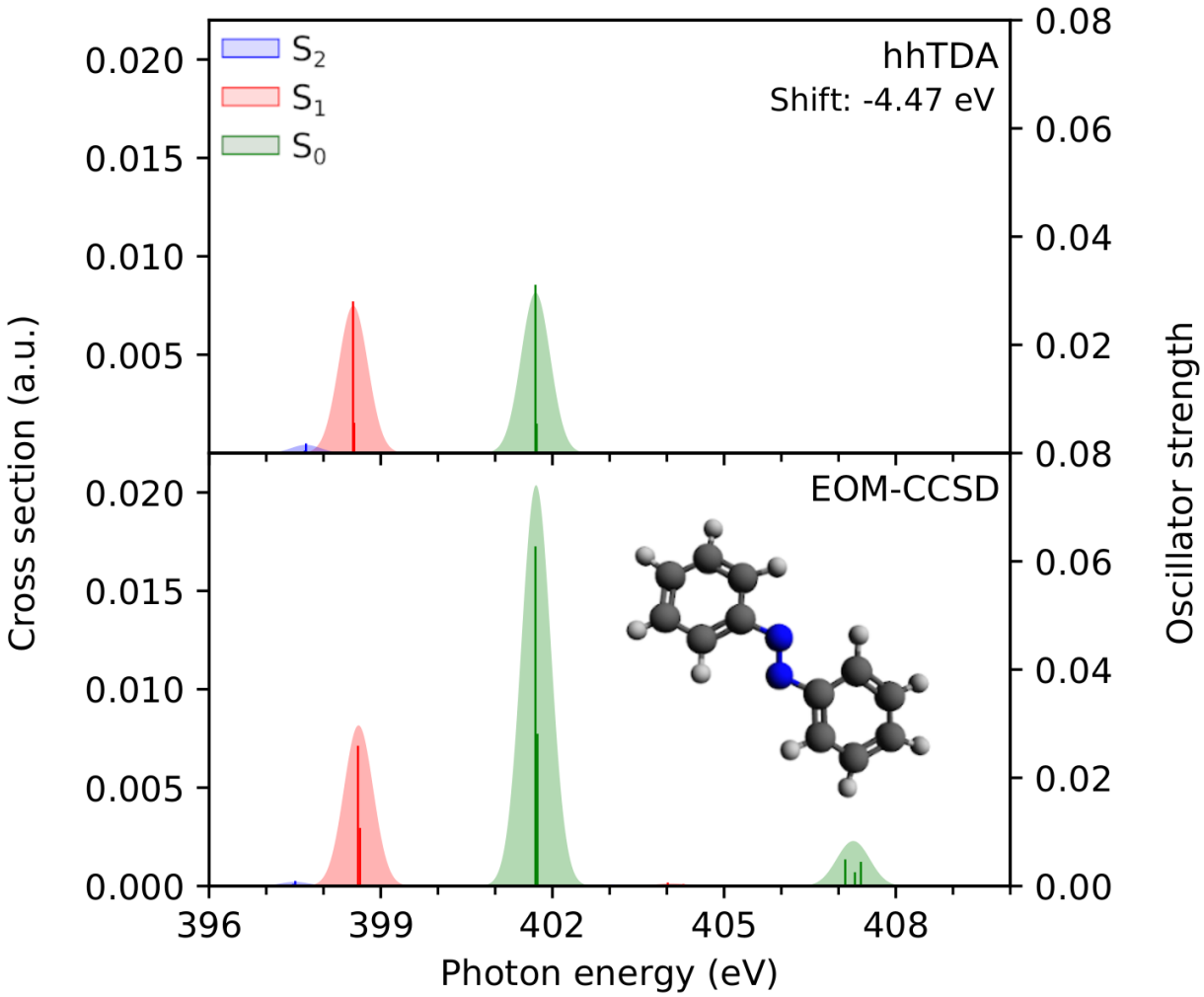


**Figure 4.** Comparison of X-ray absorption at the nitrogen K-edge of azobenzene computed with (a) CCSD/aug-cc-pCVDZ and (b) *hh*-TDA/cc-pCVDZ. Spectra are broadened with a Gaussian lineshape with full-width half maximum of 0.6 eV. The core-excitation energies are computed at the $S_0$ minimum geometry of azobenzene (in green). In blue and red, respectively, the excited-state absorption from the $S_1$ and $S_2$ states is shown. The *hh*-TDA excitation energies are shifted so that the first core excitation from the $S_0$ state between *hh*-TDA and CCSD is brought into agreement.

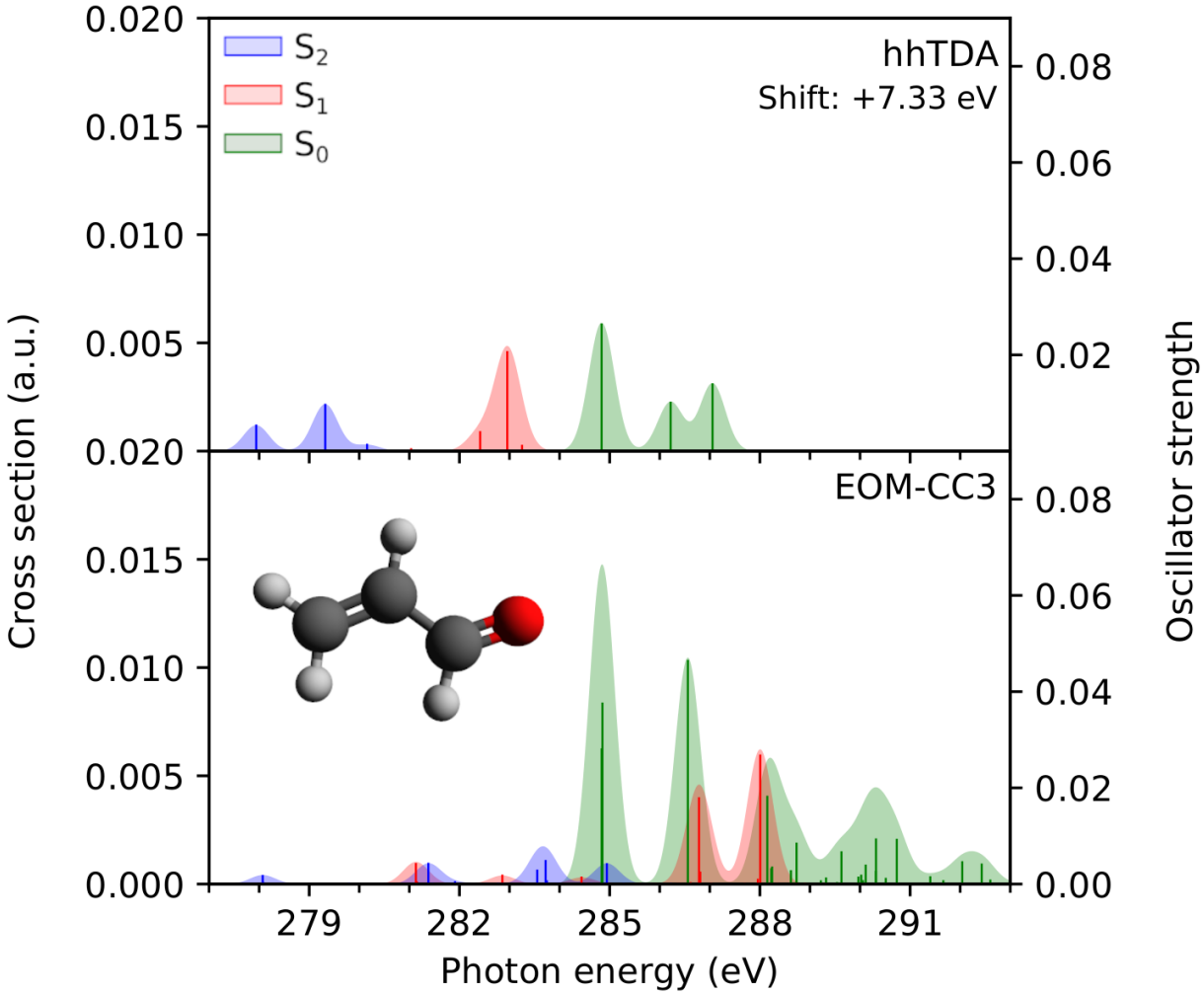


**Figure 5.** Comparison of X-ray absorption at the carbon K-edge of acrolein computed with (a) CC3/aug-cc-p(C)VTZ and (b) *hh*-TDA/cc-pCVDZ. Spectra are broadened with a Gaussian lineshape with full-width half maximum of 0.6 eV. The core-excitation energies are computed at the $S_0$ minimum geometry of acrolein (in green). In blue and red, respectively, the excited-state absorption from the $S_1$ and $S_2$ states is shown. The *hh*-TDA excitation energies are shifted so that the first core excitation from the $S_0$ state between *hh*-TDA and CCSD is brought into agreement.

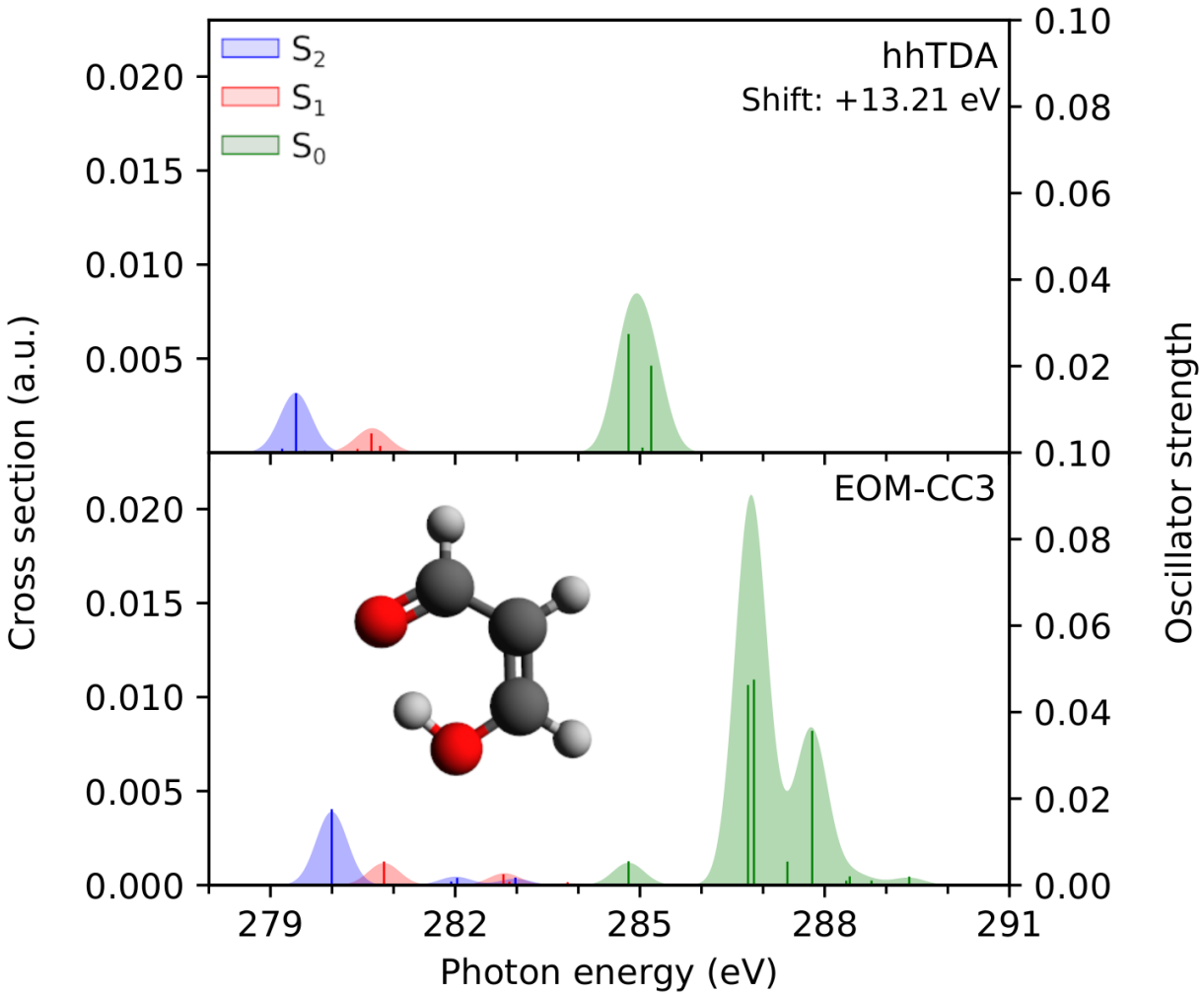


**Figure 6.** Comparison of X-ray absorption at the carbon K-edge of malonaldehyde computed with (a) CC3/aug-cc-p(C)VTZ and (b) *hh*-TDA/cc-pCVDZ. Spectra are broadened with a Gaussian lineshape with full-width half maximum of 0.6 eV. The core-excitation energies are computed at the $S_0$ minimum geometry of malonaldehyde (in green). In blue and red, respectively, the excited-state absorption from the $S_1$ and $S_2$ states is shown. The *hh*-TDA excitation energies are shifted so that the first core excitation from the $S_0$ state between *hh*-TDA and CCSD is brought into agreement.

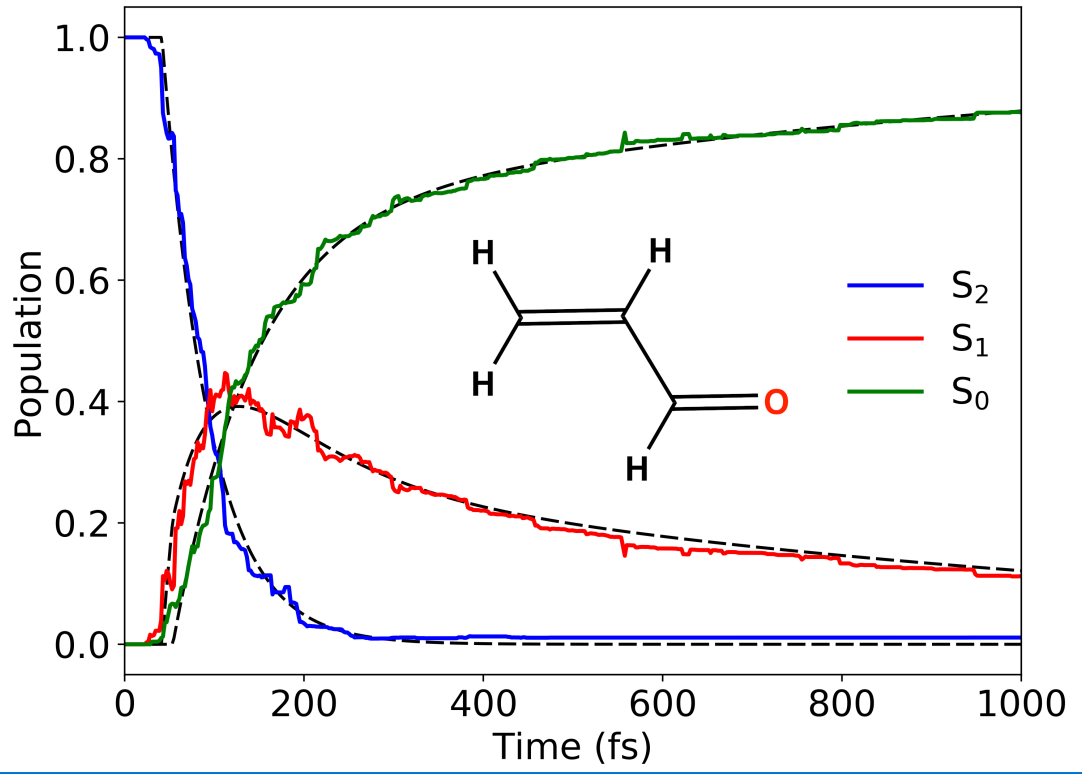


**Figure 7.** Population of the adiabatic singlet electronic states of acrolein following photoexcitation to the $S_2$ state. The $S_2$ state exhibits delayed exponential decay with an onset time constant: $t_0$ = 42 fs and decay constant: $\tau_1$ = 52 fs. The recovery of the ground state is characterized by a delayed bi-exponential with an onset time constant: $t_0$ = 54 fs and decay constants of $\tau_1$ = 90 fs for the fast component and $\tau_2$ = 1.1 ps for the slow component.

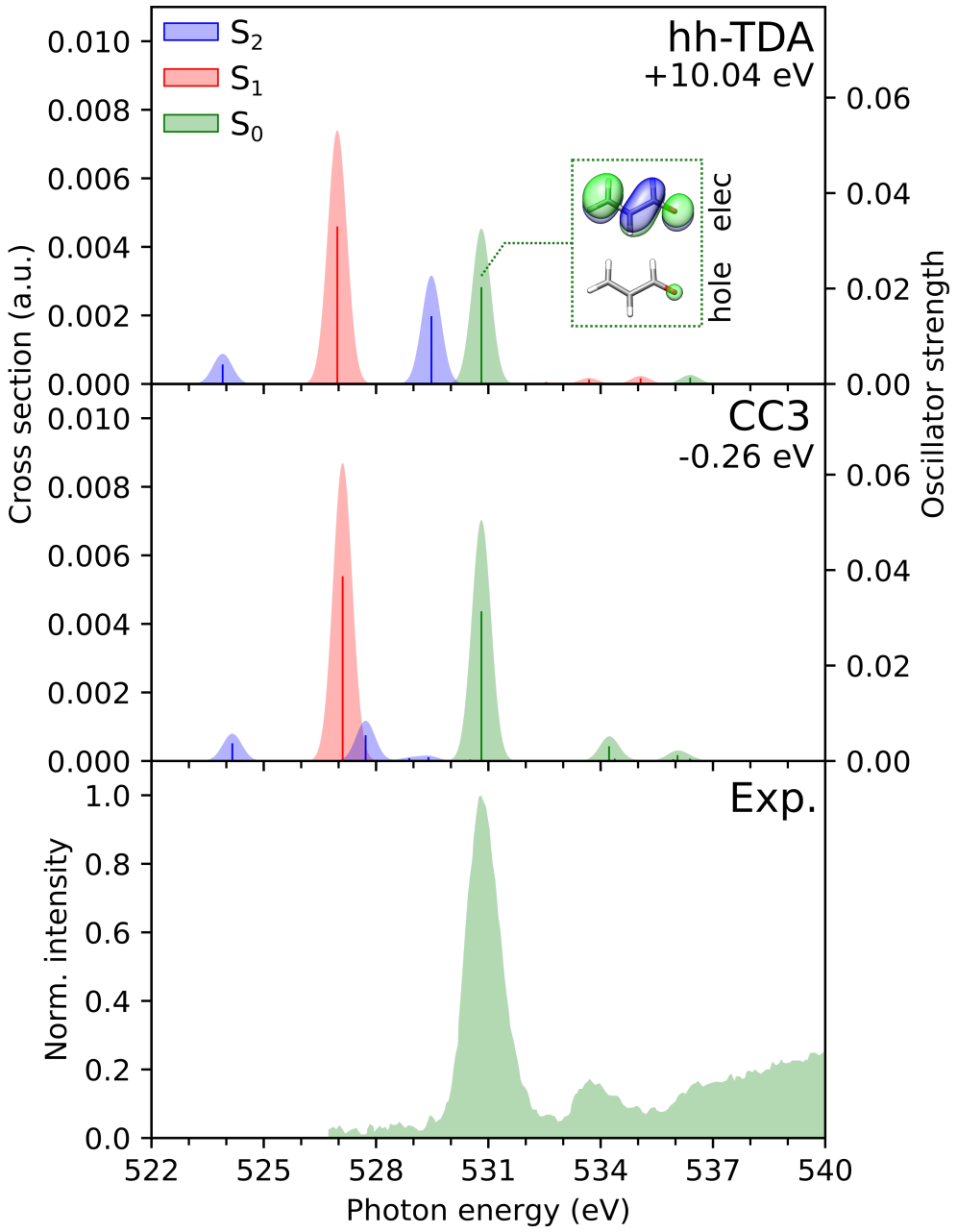


**Figure 8.** Comparison of X-ray absorption at the oxygen K-edge of acrolein computed with *hh*-TDA (upper panel), CC3 (middle panel) and the experimental spectrum[81] is shown in the lower panel. Spectra are broadened with a Gaussian lineshape with full-width half maximum of 0.6 eV. The ground state absorption at the $S_0$ minimum is shown in green. Shown in red and blue is the excited-state absorption from the $S_1$ and $S_2$ states, respectively (also computed at the $S_0$ minimum). All *hh*-TDA and CC3 excitation energies were shifted by 10.04 eV and -0.26 eV, respectively, to bring them into agreement with experiment.

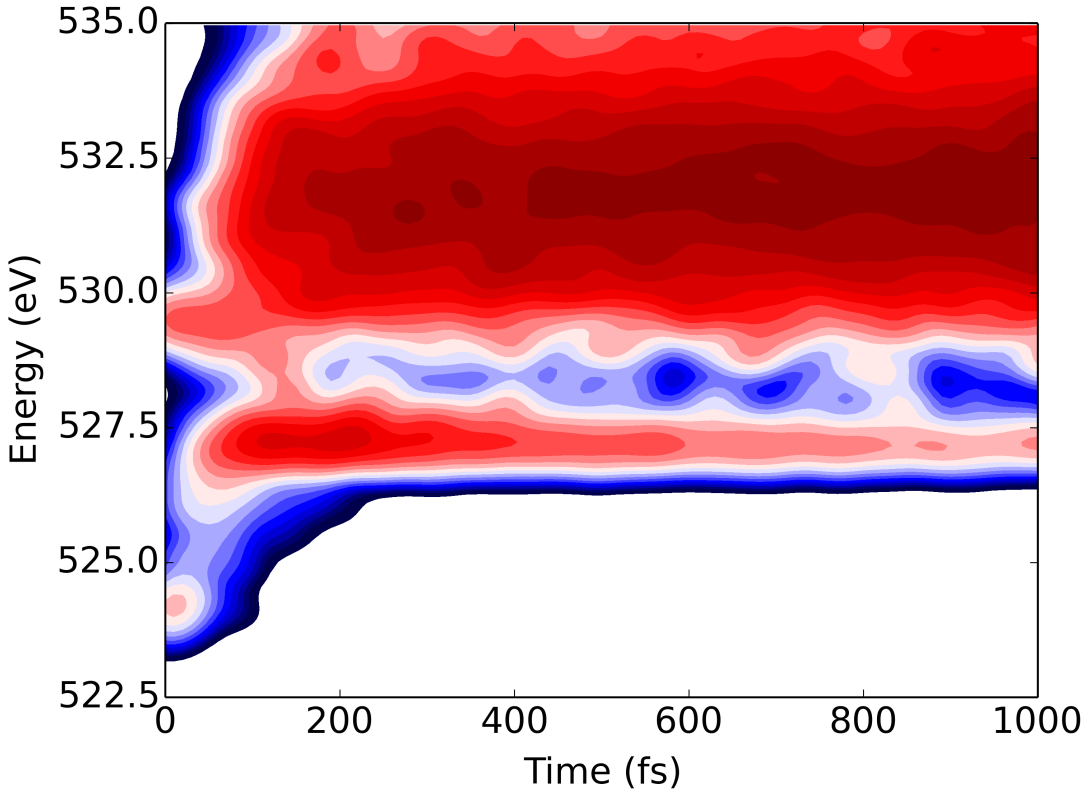


**Figure 9.** Simulated oxygen K-edge TR-NEXAFS of acrolein for 1 ps following photoexcitation to the $S_2$ state. The signal is convoluted in time with a Gaussian with full-width at half-max of 50 fs to simulate the instrument response function. A uniform spectral shift of 10.04 eV was applied to all *hh*-TDA excitation energies. Here, red signifies regions with the highest absorption and blue is the lowest absorption.

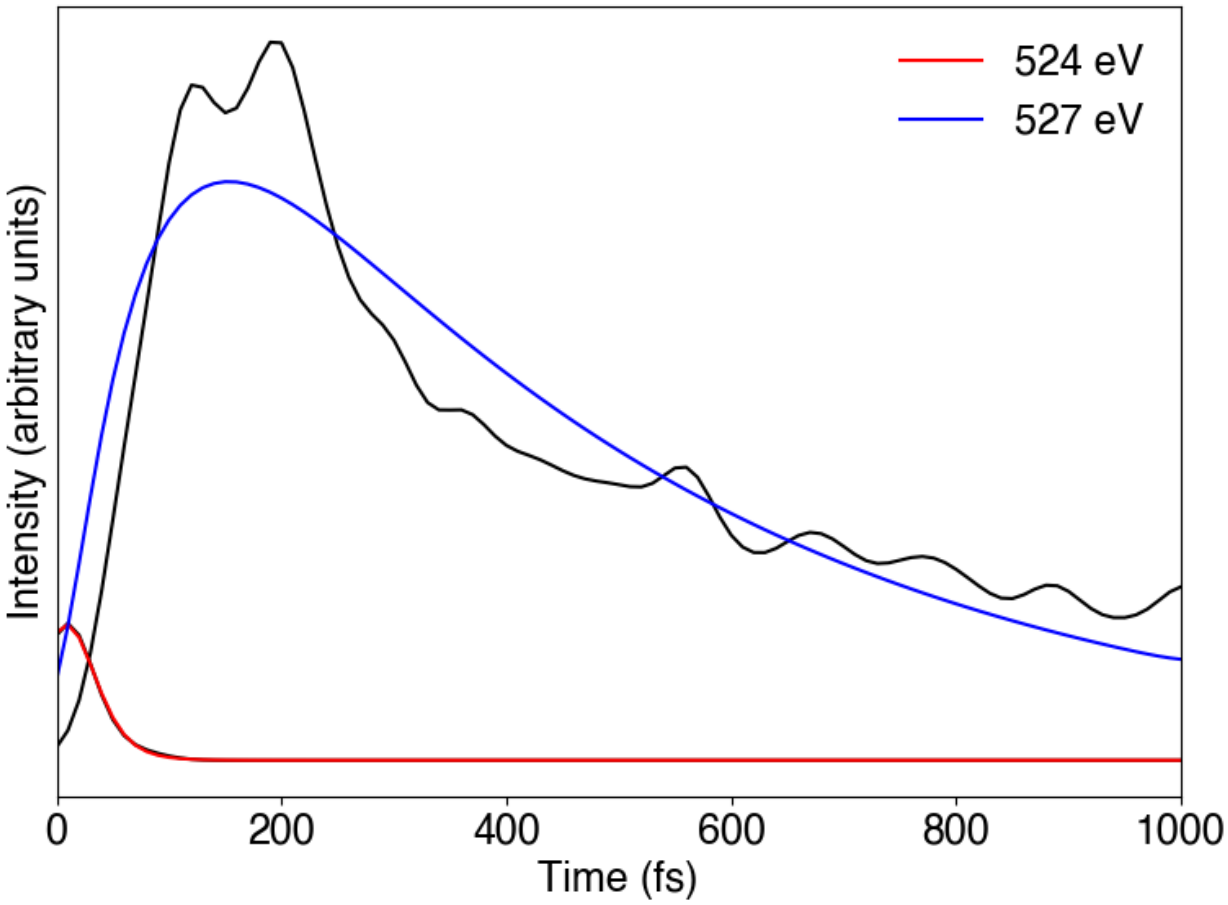


**Figure 10.** A sequential kinetics model of the dynamics of acrolein fit to lineouts from the simulated oxygen K-edge TR-NEXAFS of acrolein. The Gaussian convolution in time (full-width at half-max of 50 fs) and the spectral shift of 10.04 eV follows from the simulated TR-NEXAFS spectrum. The decay of the signal at 524 eV has a time constant of 20 fs. The rise of the signal at 527 eV has a time constant of 70 fs and the decay of that signal has a time constant of 440 fs.

**REFERENCES**


1. Zewail, A. H., Femtochemistry: Atomic-scale dynamics of the chemical bond. *J. Phys. Chem. A* **2000,** *104* (24), 5660-5694.
2. Larsson, M., Nobel Symposium on Free Electron Laser Research. *Appl. Sci.* **2017,** *7* (4), 408.
3. Young, L.; Ueda, K.; Guhr, M.; Bucksbaum, P. H.; Simon, M.; Mukamel, S.; Rohringer, N.; Prince, K. C.; Masciovecchio, C.; Meyer, M.; Rudenko, A.; Rolles, D.; Bostedt, C.; Fuchs, M.; Reis, D. A.; Santra, R.; Kapteyn, H.; Murnane, M.; Ibrahim, H.; Legare, F.; Vrakking, M.; Isinger, M.; Kroon, D.; Gisselbrecht, M.; L'Huillier, A.; Worner, H. J.; Leone, S. R., Roadmap of ultrafast x-ray atomic and molecular physics. *J. Phys. B* **2018,** *51* (3), 032003.
4. Gühr, M., Ultrafast Soft X-ray Probing of Gas Phase Molecular Dynamics. *Synchrotron Radiat. News* **2016,** *29* (5), 8-12.
5. Stöhr, J., *NEXAFS Spectroscopy*. Springer-Verlag: Berlin Heidelberg, 1992.
6. Attar, A. R.; Bhattacherjee, A.; Pemmaraju, C. D.; Schnorr, K.; Closser, K. D.; Prendergast, D.; Leone, S. R., Femtosecond x-ray spectroscopy of an electrocyclic ring-opening reaction. *Science* **2017,** *356* (6333), 54-58.
7. Erk, B.; Boll, R.; Trippel, S.; Anielski, D.; Foucar, L.; Rudek, B.; Epp, S. W.; Coffee, R.; Carron, S.; Schorb, S.; Ferguson, K. R.; Swiggers, M.; Bozek, J. D.; Simon, M.; Marchenko, T.; Küpper, J.; Schlichting, I.; Ullrich, J.; Bostedt, C.; Rolles, D.; Rudenko, A., Imaging charge transfer in iodomethane upon x-ray photoabsorption. *Science* **2014,** *345* (6194), 288.
8. McFarland, B. K.; Farrell, J. P.; Miyabe, S.; Tarantelli, F.; Aguilar, A.; Berrah, N.; Bostedt, C.; Bozek, J. D.; Bucksbaum, P. H.; Castagna, J. C.; Coffee, R. N.; Cryan, J. P.; Fang, L.; Feifel, R.; Gaffney, K. J.; Glownia, J. M.; Martinez, T. J.; Mucke, M.; Murphy, B.; Natan, A.; Osipov, T.; Petrovic, V. S.; Schorb, S.; Schultz, T.; Spector, L. S.; Swiggers, M.; Tenney, I.; Wang, S.; White, J. L.; White, W.; Guhr, M., Ultrafast X-ray Auger probing of photoexcited molecular dynamics. *Nature Comm.* **2014,** *5*, 4235.
9. Petrović, V. S.; Siano, M.; White, J. L.; Berrah, N.; Bostedt, C.; Bozek, J. D.; Broege, D.; Chalfin, M.; Coffee, R. N.; Cryan, J.; Fang, L.; Farrell, J. P.; Frasinski, L. J.; Glownia, J. M.; Gühr, M.; Hoener, M.; Holland, D. M. P.; Kim, J.; Marangos, J. P.; Martinez, T.; McFarland, B. K.; Minns, R. S.; Miyabe, S.; Schorb, S.; Sension, R. J.; Spector, L. S.; Squibb, R.; Tao, H.; Underwood, J. G.; Bucksbaum, P. H., Transient X-Ray Fragmentation: Probing a Prototypical Photoinduced Ring Opening. *Phys. Rev. Lett.* **2012,** *108* (25), 253006.
10. Wolf, T. J. A.; Myhre, R. H.; Cryan, J. P.; Coriani, S.; Squibb, R. J.; Battistoni, A.; Berrah, N.; Bostedt, C.; Bucksbaum, P.; Coslovich, G.; Feifel, R.; Gaffney, K. J.; Grilj, J.; Martinez, T. J.; Miyabe, S.; Moeller, S. P.; Mucke, M.; Natan, A.; Obaid, R.; Osipov, T.; Plekan, O.; Wang, S.; Koch, H.; Guhr, M., Probing ultrafast pi pi*/n pi* internal conversion in organic chromophores via K-edge resonant absorption. *Nature Comm.* **2017,** *8*, 29.
11. Neville, S. P.; Averbukh, V.; Ruberti, M.; Yun, R.; Patchkovskii, S.; Chergui, M.; Stolow, A.; Schuurman, M. S., Excited state X-ray absorption spectroscopy: Probing both electronic and structural dynamics. *J. Chem. Phys.* **2016,** *145* (14), 144307.
12. Ehlert, C.; Gühr, M.; Saalfrank, P., An efficient first principles method for molecular pump-probe NEXAFS spectra: Application to thymine and azobenzene. *J. Chem. Phys.* **2018,** *149* (14), 144112.

13. Neville, S. P.; Chergui, M.; Stolow, A.; Schuurman, M. S., Ultrafast X-Ray Spectroscopy of Conical Intersections. *Phys. Rev. Lett.* **2018,** *120* (24), 243001.
14. Northey, T.; Duffield, J.; Penfold, T. J., Non-equilibrium x-ray spectroscopy using direct quantum dynamics. *J. Chem. Phys.* **2018,** *149* (12), 124107.
15. Vaz da Cruz, V.; Ignatova, N.; Couto, R. C.; Fedotov, D. A.; Rehn, D. R.; Savchenko, V.; Norman, P.; Ågren, H.; Polyutov, S.; Niskanen, J.; Eckert, S.; Jay, R. M.; Fondell, M.; Schmitt, T.; Pietzsch, A.; Föhlisch, A.; Gel'mukhanov, F.; Odelius, M.; Kimberg, V., Nuclear dynamics in resonant inelastic X-ray scattering and X-ray absorption of methanol. *J. Chem. Phys.* **2019,** *150* (23), 234301.
16. Segatta, F.; Nenov, A.; Orlandi, S.; Arcioni, A.; Mukamel, S.; Garavelli, M., Exploring the capabilities of optical pump X-ray probe NEXAFS spectroscopy to track photo-induced dynamics mediated by conical intersections. *Faraday Discuss.* **2020,** *221* (0), 245-264.
17. Neville, S. P.; Averbukh, V.; Patchkovskii, S.; Ruberti, M.; Yun, R.; Chergui, M.; Stolow, A.; Schuurman, M. S., Beyond structure: ultrafast X-ray absorption spectroscopy as a probe of non-adiabatic wavepacket dynamics. *Faraday Discuss.* **2016,** *194* (0), 117-145.
18. Northey, T.; Norell, J.; Fouda, A. E. A.; Besley, N. A.; Odelius, M.; Penfold, T. J., Ultrafast nonadiabatic dynamics probed by nitrogen K-edge absorption spectroscopy. *Phys. Chem. Chem. Phys.* **2020**.
19. List, N. H.; Dempwolff, A. L.; Dreuw, A.; Norman, P.; Martínez, T. J., Probing competing relaxation pathways in malonaldehyde with transient X-ray absorption spectroscopy. *Chemical Science* **2020,** *11* (16), 4180-4193.
20. Bernardi, F.; Olivucci, M.; Robb, M. A., Potential energy surface crossings in organic photochemistry. *Chem. Soc. Rev.* **1996,** *25* (5), 321-&.
21. Levine, B. G.; Martinez, T. J., Isomerization through conical intersections. *Ann. Rev. Phys. Chem.* **2007,** *58*, 613-634.
22. Plasser, F.; Barbatti, M.; Aquino, A. J. A.; Lischka, H., Electronically excited states and photodynamics: a continuing challenge. *Theor. Chem. Acc.* **2012,** *131* (1).
23. Cederbaum, L. S.; Domcke, W.; Schirmer, J., Many-Body Theory of Core Holes. *Phys. Rev. A* **1980,** *22* (1), 206-222.
24. Barth, A.; Cederbaum, L. S., Many-Body Theory of Core-Valence Excitations. *Phys. Rev. A* **1981,** *23* (3), 1038-1061.
25. Tsuru, S.; Vidal, M. L.; Pápai, M.; Krylov, A. I.; Møller, K. B.; Coriani, S., Time-resolved near-edge X-ray absorption fine structure of pyrazine from electronic structure and nuclear wave packet dynamics simulations. *J. Chem. Phys.* **2019,** *151* (12), 124114.
26. Besley, N. A., Equation of motion coupled cluster theory calculations of the X-ray emission spectroscopy of water. *Chem. Phys. Lett.* **2012,** *542*, 42-46.
27. Coriani, S.; Christiansen, O.; Fransson, T.; Norman, P., Coupled-cluster response theory for near-edge x-ray-absorption fine structure of atoms and molecules. *Phys. Rev. A* **2012,** *85* (2), 022507.
28. Fransson, T.; Coriani, S.; Christiansen, O.; Norman, P., Carbon X-ray absorption spectra of fluoroethenes and acetone: A study at the coupled cluster, density functional, and static-exchange levels of theory. *J. Chem. Phys.* **2013,** *138* (12), 124311.
29. Coriani, S.; Koch, H., Communication: X-ray absorption spectra and core-ionization potentials within a core-valence separated coupled cluster framework. *J. Chem. Phys.* **2015,** *143* (18), 181103.

30. Peng, B.; Lestrange, P. J.; Goings, J. J.; Caricato, M.; Li, X., Energy-Specific Equation-of-Motion Coupled-Cluster Methods for High-Energy Excited States: Application to K-edge X-ray Absorption Spectroscopy. *J. Chem. Theory Comput.* **2015,** *11* (9), 4146-4153.
31. Bokhan, D.; Trubnikov, D. N.; Perera, A.; Bartlett, R. J., Explicitly-correlated double ionization potentials and double electron attachment equation-of-motion coupled cluster methods. *Chem. Phys. Lett.* **2018,** *692*, 191-195.
32. Norman, P.; Dreuw, A., Simulating X-ray Spectroscopies and Calculating Core-Excited States of Molecules. *Chem. Rev.* **2018,** *118* (15), 7208-7248.
33. Nascimento, D. R.; DePrince, A. E., Simulation of Near-Edge X-ray Absorption Fine Structure with Time-Dependent Equation-of-Motion Coupled-Cluster Theory. *J. Phys. Chem. Lett.* **2017,** *8* (13), 2951-2957.
34. Stanton, J. F.; Bartlett, R. J., The Equation of Motion Coupled-Cluster Method. A Systematic Biorthogonal Approach to Molecular-Excitation Energies, Transition-Probabilities, and Excited-State Properties. *J. Chem. Phys.* **1993,** *98* (9), 7029-7039.
35. Wolf, T. J. A.; Myhre, R. H.; Cryan, J. P.; Coriani, S.; Squibb, R. J.; Battistoni, A.; Berrah, N.; Bostedt, C.; Bucksbaum, P.; Coslovich, G.; Feifel, R.; Gaffney, K. J.; Grilj, J.; Martinez, T. J.; Miyabe, S.; Moeller, S. P.; Mucke, M.; Natan, A.; Obaid, R.; Osipov, T.; Plekan, O.; Wang, S.; Koch, H.; Guhr, M., Probing ultrafast pi pi*/n pi* internal conversion in organic chromophores via K-edge resonant absorption. *Nat. Commun.* **2017,** *8*.
36. Myhre, R. H.; Wolf, T. J. A.; Cheng, L.; Nandi, S.; Coriani, S.; Gühr, M.; Koch, H., A theoretical and experimental benchmark study of core-excited states in nitrogen. *J. Chem. Phys.* **2018,** *148* (6), 064106.
37. Carbone, J. P.; Cheng, L.; Myhre, R. H.; Matthews, D.; Koch, H.; Coriani, S., Chapter Eleven - An analysis of the performance of coupled cluster methods for K-edge core excitations and ionizations using standard basis sets. In *Advances in Quantum Chemistry*, Ancarani, L. U.; Hoggan, P. E., Eds. Academic Press: 2019; Vol. 79, pp 241-261.
38. Kjønstad, E. F.; Koch, H., Resolving the Notorious Case of Conical Intersections for Coupled Cluster Dynamics. *J. Phys. Chem. Lett.* **2017,** *8* (19), 4801-4807.
39. Köhn, A.; Tajti, A., Can coupled-cluster theory treat conical intersections? *J. Chem. Phys.* **2007,** *127* (4), 044105.
40. Kjonstad, E. F.; Myhre, R. H.; Martinez, T. J.; Koch, H., Crossing conditions in coupled cluster theory. *J. Chem. Phys.* **2017,** *147*, 164105.
41. Malmqvist, P. Å.; Pierloot, K.; Shahi, A. R. M.; Cramer, C. J.; Gagliardi, L., The restricted active space followed by second-order perturbation theory method: Theory and application to the study of CuO2 and Cu2O2 systems. *J. Chem. Phys.* **2008,** *128* (20), 204109.
42. Huber, S. M.; Moughal Shahi, A. R.; Aquilante, F.; Cramer, C. J.; Gagliardi, L., What Active Space Adequately Describes Oxygen Activation by a Late Transition Metal? CASPT2 and RASPT2 Applied to Intermediates from the Reaction of O2 with a Cu(I)-α-Ketocarboxylate. *J. Chem. Theory Comput.* **2009,** *5* (11), 2967-2976.
43. Sauri, V.; Serrano-Andrés, L.; Shahi, A. R. M.; Gagliardi, L.; Vancoillie, S.; Pierloot, K., Multiconfigurational Second-Order Perturbation Theory Restricted Active Space (RASPT2) Method for Electronic Excited States: A Benchmark Study. *J. Chem. Theory Comput.* **2011,** *7* (1), 153-168.
44. Josefsson, I.; Kunnus, K.; Schreck, S.; Föhlisch, A.; de Groot, F.; Wernet, P.; Odelius, M., Ab Initio Calculations of X-ray Spectra: Atomic Multiplet and Molecular Orbital Effects in a

Multiconfigurational SCF Approach to the L-Edge Spectra of Transition Metal Complexes. *J. Phys. Chem. Lett.* **2012,** *3* (23), 3565-3570.
45. Pinjari, R. V.; Delcey, M. G.; Guo, M.; Odelius, M.; Lundberg, M., Restricted active space calculations of L-edge X-ray absorption spectra: From molecular orbitals to multiplet states. *J. Chem. Phys.* **2014,** *141* (12), 124116.
46. Guo, M.; Källman, E.; Sørensen, L. K.; Delcey, M. G.; Pinjari, R. V.; Lundberg, M., Molecular Orbital Simulations of Metal 1s2p Resonant Inelastic X-ray Scattering. *J. Phys. Chem. A* **2016,** *120* (29), 5848-5855.
47. Guo, M.; Sørensen, L. K.; Delcey, M. G.; Pinjari, R. V.; Lundberg, M., Simulations of iron K pre-edge X-ray absorption spectra using the restricted active space method. *Phys. Chem. Chem. Phys.* **2016,** *18* (4), 3250-3259.
48. Pinjari, R. V.; Delcey, M. G.; Guo, M.; Odelius, M.; Lundberg, M., Cost and sensitivity of restricted active-space calculations of metal L-edge X-ray absorption spectra. *J. Comput. Chem.* **2016,** *37* (5), 477-486.
49. Källman, E.; Guo, M.; Delcey, M. G.; Meyer, D. A.; Gaffney, K. J.; Lindh, R.; Lundberg, M., Simulations of valence excited states in coordination complexes reached through hard X-ray scattering. *Phys. Chem. Chem. Phys.* **2020,** *22* (16), 8325-8335.
50. Levine, B. G.; Ko, C.; Quenneville, J.; Martinez, T. J., Conical intersections and double excitations in time-dependent density functional theory. *Mol. Phys.* **2006,** *104* (5-7), 1039-1051.
51. Koslowski, A.; Beck, M. E.; Thiel, W., Implementation of a general multireference configuration interaction procedure with analytic gradients in a semiempirical context using the graphical unitary group approach. *J. Comput. Chem.* **2003,** *24* (6), 714-726.
52. Dral, P. O.; Wu, X.; Spörkel, L.; Koslowski, A.; Weber, W.; Steiger, R.; Scholten, M.; Thiel, W., Semiempirical Quantum-Chemical Orthogonalization-Corrected Methods: Theory, Implementation, and Parameters. *J. Chem. Theory Comput.* **2016,** *12* (3), 1082-1096.
53. Toniolo, A.; Thompson, A. L.; Martinez, T. J., Excited state dynamics of benzene with reparameterized multi-reference semiempirical configuration interaction methods. *Chem. Phys.* **2004,** *304*, 133-145.
54. Toniolo, A.; Olsen, S.; Manohar, L.; Martinez, T. J., Conical intersection dynamics in solution: The chromophore of Green Fluorescent Protein. *Faraday Disc.* **2004,** *127*, 149-163.
55. Toniolo, A.; Ciminelli, C.; Persico, M.; Martinez, T. J., Simulation of the photodynamics of azobenzene on its first excited state: Comparison of full multiple spawning and surface hopping treatments. *J. Chem. Phys.* **2005,** *123*, 234308.
56. Bannwarth, C.; Yu, J. K.; Hohenstein, E. G.; Martinez, T. J., Hole-hole Tamm-Dancoff-approximated density functional theory: A highly efficient electronic structure method incorporating dynamic and static correlation. *J. Chem. Phys.* **2020,** *153*, 024110.
57. Yu, J. K.; Bannwarth, C.; Hohenstein, E. G.; Martinez, T. J., Ab Initio Nonadiabatic Molecular Dynamics with Hole-Hole Tamm-Dancoff Approximated Density Functional Theory. *J Chem Theory Comput* **2020,** *16* (9), 5499-5511.
58. Scuseria, G. E.; Henderson, T. M.; Bulik, I. W., Particle-particle and quasiparticle random phase approximations: Connections to coupled cluster theory. *J. Chem. Phys.* **2013,** *139*, 104113.
59. Zhang, D.; Peng, D.; Zhang, P.; Yang, W., Analytic gradients, geometry optimization and excited state potential energy surfaces from the particle-particle random phase approximation. *Phys. Chem. Chem. Phys.* **2015,** *17*, 1025-1038.

60. Yang, Y.; cvan Aggelen, H.; Yang, W., Double, Rydberg and charge transfer excitations from pairing matrix fluctuation and particle-particle random phase approximation. *J. Chem. Phys.* **2013,** *139*, 224105.
61. Yu, J. K.; Bannwarth, C.; Liang, R.; Hohenstein, E. G.; Martínez, T. J., Nonadiabatic Dynamics Simulation of the Wavelength-Dependent Photochemistry of Azobenzene Excited to the nπ* and ππ* Excited States. *J. Am. Chem. Soc.* **2020,** *142* (49), 20680-20690.
62. Reguero, M.; Olivucci, M.; Bernardi, F.; Robb, M. A., Excited-State Potential Surface Crossings in Acrolein: A Model for Understanding the Photochemistry and Photophysics of .alpha.,.beta.-Enones. *J. Am. Chem. Soc.* **1994,** *116* (5), 2103-2114.
63. Ufimtsev, I. S.; Martínez, T. J., Quantum Chemistry on Graphical Processing Units. 1. Strategies for Two-Electron Integral Evaluation. *J. Chem. Theory Comput.* **2008,** *4* (2), 222-231.
64. Ufimtsev, I. S.; Martinez, T. J., Quantum Chemistry on Graphical Processing Units. 2. Direct Self-Consistent-Field Implementation. *J. Chem. Theory Comput.* **2009,** *5* (4), 1004-1015.
65. Ufimtsev, I. S.; Martinez, T. J., Quantum Chemistry on Graphical Processing Units. 3. Analytical Energy Gradients, Geometry Optimization, and First Principles Molecular Dynamics. *J. Chem. Theory Comput.* **2009,** *5* (10), 2619-2628.
66. Seritan, S.; Bannwarth, C.; Fales, B. S.; Hohenstein, E. G.; Kokkila-Schumacher, S. I. L.; Luehr, N.; Snyder, J. W., Jr.; Song, C.; Titov, A. V.; Ufimtsev, I. S.; Martinez, T. J., TeraChem: Accelerating electronic structure and ab initio molecular dynamics with graphical processing units. *J Chem Phys* **2020,** *152* (22), 224110.
67. Rohrdanz, M. A.; Martins, K. M.; Herbert, J. M., A long-range-corrected density functional that performs well for both ground-state properties and time-dependent density functional theory excitation energies, including charge-transfer excited states. *J. Chem. Phys.* **2009,** *130* (5).
68. Ben-Nun, M.; Quenneville, J.; Martinez, T. J., Ab initio multiple spawning: Photochemistry from first principles quantum molecular dynamics. *J. Phys. Chem. A* **2000,** *104* (22), 5161-5175.
69. Koch, H.; Christiansen, O.; Jo/rgensen, P.; Sanchez de Merás, A. M.; Helgaker, T., The CC3 model: An iterative coupled cluster approach including connected triples. *J. Chem. Phys.* **1997,** *106* (5), 1808-1818.
70. Paul, A. C.; Myhre, R. H.; Koch, H., A new and efficient implementation of CC3. *to be submitted*.
71. Folkestad, S. D.; Kjønstad, E. F.; Myhre, R. H.; Andersen, J. H.; Balbi, A.; Coriani, S.; Giovannini, T.; Goletto, L.; Haugland, T. S.; Hutcheson, A.; Høyvik, I.-M.; Moitra, T.; Paul, A. C.; Scavino, M.; Skeidsvoll, A. S.; Tveten, Å. H.; Koch, H., eT 1.0: An open source electronic structure program with emphasis on coupled cluster and multilevel methods. *J. Chem. Phys.* **2020,** *152* (18), 184103.
72. Coriani, S.; Koch, H., Erratum: "Communication: X-ray absorption spectra and core-ionization potentials within a core-valence separated coupled cluster framework" [J. Chem. Phys. 143, 181103 (2015)]. *J. Chem. Phys.* **2016,** *145* (14), 149901.
73. Fales, B. S.; Curtis, E. R.; Johnson, K. G.; Lahana, D.; Seritan, S.; Wang, Y.; Weir, H.; Martinez, T. J.; Hohenstein, E. G., Performance of Coupled-Cluster Singles and Doubles on Modern Stream Processing Architectures. *J Chem Theory Comput* **2020,** *16* (7), 4021-4028.
74. Paulisse, K. W.; Friday, T. O.; Graske, M. L.; Polik, W. F., Vibronic spectroscopy and lifetime of S1 acrolein. *J. Chem. Phys.* **2000,** *113* (1), 184-191.

75. Lee, A. M. D.; Coe, J. D.; Ullrich, S.; Ho, M. L.; Lee, S. J.; Cheng, B. M.; Zgierski, M. Z.; Chen, I. C.; Martinez, T. J.; Stolow, A., Substituent Effects on Dynamics at Conical Intersections: α,β-Enones. *J. Phys. Chem. A* **2007,** *111* (47), 11948-11960.
76. Duris, J.; Li, S.; Driver, T.; Champenois, E. G.; MacArthur, J. P.; Lutman, A. A.; Zhang, Z.; Rosenberger, P.; Aldrich, J. W.; Coffee, R.; Coslovich, G.; Decker, F.-J.; Glownia, J. M.; Hartmann, G.; Helml, W.; Kamalov, A.; Knurr, J.; Krzywinski, J.; Lin, M.-F.; Marangos, J. P.; Nantel, M.; Natan, A.; O'Neal, J. T.; Shivaram, N.; Walter, P.; Wang, A. L.; Welch, J. J.; Wolf, T. J. A.; Xu, J. Z.; Kling, M. F.; Bucksbaum, P. H.; Zholents, A.; Huang, Z.; Cryan, J. P.; Marinelli, A., Tunable isolated attosecond X-ray pulses with gigawatt peak power from a free-electron laser. *Nature Photonics* **2020,** *14* (1), 30-36.
77. Walsh, A. D., The absorption spectra of acrolein, crotonaldehyde and mesityl oxide in the vacuum ultra-violet. *Transactions of the Faraday Society* **1945,** *41* (0), 498-505.
78. Birge, R. R.; Pringle, W. C.; Leermakers, P. A., Excited-state geometries of the singly substituted methylpropenals. I. Vibrational-electronic analysis of S1(n,.pi.*). *J. Amer. Chem. Soc.* **1971,** *93* (25), 6715-6726.
79. Birge, R. R.; Leermakers, P. A., Excited-state geometries of the singly substituted methylpropenals. II. Bond order reversal and substituent interaction in S1(n,.pi.*). *J. Amer. Chem. Soc.* **1971,** *93* (25), 6726-6733.
80. Aquilante, F.; Barone, V.; Roos, B. O., A theoretical investigation of valence and Rydberg electronic states of acrolein. *J. Chem. Phys.* **2003,** *119* (23), 12323-12334.
81. Duflot, D.; Flament, J. P.; Walker, I. C.; Heinesch, J.; Hubin-Franskin, M. J., Core shell excitation of 2-propenal (acrolein) at the O 1s and C 1s edges: An experimental and ab initio study. *J. Chem. Phys.* **2003,** *118* (3), 1137-1145.